HHS Public Access

Author manuscript

Oncogene. Author manuscript; available in PMC 2020 April 21.

Published in final edited form as:

Oncogene. 2020 February ; 39(6): 1318–1334. doi:10.1038/s41388-019-1064-3.

PREX1 drives spontaneous bone dissemination of ER+ breast cancer cells

Miranda E. Clements[1,2], **Rachelle W. Johnson**[*,1,2,3]

[1]Program in Cancer Biology, Vanderbilt University, Nashville, TN, 37232

[2]Vanderbilt Center for Bone Biology, Department of Medicine, Division of Clinical Pharmacology, Vanderbilt University Medical Center, Nashville, TN 37232

[3]Department of Medicine, Division of Clinical Pharmacology, Vanderbilt University Medical Center, Nashville, TN, 37232

Abstract

A significant proportion of breast cancer patients develop bone metastases, but the mechanisms regulating tumor cell dissemination from the primary site to the skeleton remain largely unknown. Using a novel model of spontaneous bone metastasis derived from human ER+ MCF7 cells, molecular profiling revealed increased PREX1 expression in a cell line established from bone-disseminated MCF7 cells (MCF7b), which were more migratory, invasive, and adhesive *in vitro* compared to parental MCF7 cells, and this phenotype was mediated by PREX1. MCF7b cells grew poorly in the primary tumor site when re-inoculated *in vivo*, suggesting these cells are primed to grow in the bone, and were enriched in skeletal sites of metastasis over soft tissue sites. Skeletal dissemination from the primary tumor was reversed with PREX1 knockdown, indicating that PREX1 is a key driver of spontaneous dissemination of tumor cells from the primary site to the bone marrow. In breast cancer patients, PREX1 levels are significantly increased in ER+ tumors and associated with invasive disease and distant metastasis. Together, these findings implicate PREX1 in spontaneous bone dissemination and provide a significant advance to the molecular mechanisms by which breast cancer cells disseminate from the primary tumor site to bone.

Introduction

Despite advances in early diagnosis and treatment, relapse occurs in approximately 20–30% of breast cancer patients [1]. The most frequent and often first site of metastasis in breast cancer patients is the bone, which results in significant morbidities including bone pain, hypercalcemia, and fractures [2, 3]. Nearly 80% of breast cancer patients who succumb to

[*]Corresponding author: Rachelle W. Johnson, 2215b Garland Ave, 1165C Medical Research Building IV, Vanderbilt University, Nashville, TN 37232, rachelle.johnson@vumc.org, Phone: 615-875-8965.

Author Contributions: MEC and RWJ conceptualized the project, performed the experiments, wrote, edited, and reviewed the manuscript.

Competing Interests. The authors declare no competing financial interests.

disease harbor bone metastases upon autopsy, suggesting patients are at significant risk of developing distant metastasis [4, 5]. Estrogen receptor positive (ER+) tumors, which comprise approximately 70% of all breast cancers, have a greater propensity to metastasize to bone than the visceral organs [6]. Further, patients with ER+ disease exhibit prolonged latency periods prior to recurrence with bone metastases most frequently occurring 8–10 years following primary tumor diagnosis. In contrast, the development of bone metastases in ER- patients typically occurs within five years of diagnosis [7, 8]. Together, these clinical observations suggest that tumor dissemination and metastatic outgrowth may be regulated by subtype-specific mechanisms.

Metastasis is initiated by the invasion of tumor cells through the local basement membrane and survival in the circulation, followed by homing to a distant site and eventual outgrowth into a clinically detectable metastasis. Over the past decade, several groups have sought to identify molecular alterations that promote spontaneous bone metastasis using comparative gene expression analysis of tumor samples from patients with and without bone metastases [9, 10] as well as parental and bone-metastatic subclones of the MDA-MB-231 cell line [11]. These analyses have identified several gene signatures [9–11] and key signaling pathways, such as the $CXCR4^{Tumor}$ -$CXCL12^{Osteoblast}$ axis [11], that drive tumor cell homing to bone. However, these studies have predominantly focused on ER- breast cancer and have not extensively investigated the contribution of the identified genes to metastasis *in vivo*. Importantly, those mechanisms that reportedly control bone metastasis *in vivo* have predominantly been explored using intracardiac inoculation of tumor cells, which bypasses dissemination from the primary tumor and intravasation into circulation. Thus, the contribution of these factors to metastasis may be restricted to the later stages of the metastatic cascade including tumor cell homing, extravasation, or colonization of the bone. Given the limitations with current animal models, relatively few mechanisms that mediate spontaneous dissemination from the primary tumor to the bone have been identified. Further exploration into the mechanisms controlling these early stages of bone metastasis, particularly in ER+ disease, are necessary to advance the prevention and effective treatment of bone metastasis.

Members of the Rho family of small GTP-binding proteins including the Rac proteins regulate many pro-metastatic processes such as cell migration, adhesion, and cytokinesis [12]. Activation of these proteins is controlled by guanine nucleotide exchange factors (GEFs), which promote exchange of bound GDP for free GTP [12]. Overexpression of GEFs has been reported to promote tumor development and metastasis in numerous cancer types including those that commonly metastasize to bone such as breast and prostate [13, 14]. The Rac-GEF, phosphatidylinositol-3,4,5-trisphosphate dependent Rac exchange factor 1 (PREX1), is frequently upregulated in ER+ breast cancer [15, 16] and has been shown to contribute to ER+ primary tumor growth in preclinical animal models through activation of IGF-1R/InsR, Rac1, PI3K/AKT, and MEK/ERK [17, 18]. Despite its known contribution to melanoma[19] and prostate [20] metastasis, the role of PREX1 in breast cancer metastasis has not been experimentally investigated. Moreover, evaluation of PREX1 expression in breast cancer patient samples has yielded conflicting results with several studies reporting an association of high PREX1 expression with breast cancer metastasis [16, 21] and reduced disease-free survival [15] while others indicate the opposite trend [22, 23].

Here, we sought to identify factors involved in tumor cell dissemination to the skeleton using a bone-tropic mouse model derived from the human ER+ MCF7 cell line that encompasses the entire metastatic cascade *in vivo*. Our data identify PREX1 as an important mediator of breast cancer dissemination specifically to sites of the skeleton and not the lung and as such is a significant advance in our understanding of the molecular mechanisms that promote spontaneous dissemination of breast cancer cells from the primary tumor site to the bone marrow. PREX1 upregulation in ER+ breast cancer is associated with invasive disease and distant metastasis, thus highlighting the clinical importance of these findings.

Results

Establishment of a human ER+ spontaneous bone metastasis model

To identify molecular factors driving skeletal dissemination in a clinically relevant model, we implanted human ER+ MCF7 cells into the mammary fat pad of mice without estradiol supplementation to avoid well-known bone and urinary toxicities [24, 25] (Fig. 1A). Prior to inoculation parental MCF7 cells were transduced with a lentiviral vector containing GFP and a non-silencing shRNA and are hereinafter referred to as MCF7 cells. As previously reported in the absence of exogenous estradiol (19–21), palpable nodules developed, but did not progress, and in most cases dissipated. Approximately 6 months after tumor inoculation, flow cytometric analysis of the bone marrow (n=4 mice) using the epithelial cell marker, EpCAM, positively detected tumor cells in one mouse, which were sorted into single cell clones (Fig. 1A). Notably, these tumor cells no longer expressed GFP (Fig. 1A). The MCF7 bone metastatic line (MCF7b) was derived from one of these clones and was recently confirmed to be a 100% match to MCF7 cells banked at ATCC using STR profiling.

MCF7b cells exhibit enhanced metastatic potential

To establish the suitability of the MCF7b model to identify factors mediating bone metastasis, we sought to validate the enhanced metastatic potential of MCF7b cells *in vitro* and *in vivo*. Compared to the parental cell line, MCF7b cells appeared similar morphologically (Fig. 1B) and did not display an altered proliferation rate by trypan blue exclusion or CellTrace Violet dilution assays (Fig. 1C, D). Total levels and basal activity of AKT, ERK, and STAT3 were also unchanged in MCF7b cells by western blot and RPPA analysis (Fig. 1E and Fig. S1A–C).

Notably, RPPA analysis revealed that MCF7b cells maintained ERα protein levels and pS118 ERα, a post-translational modification that promotes ERα binding to ERE-containing promoters and synchronizes transcriptional activity [26–28], was also unchanged (Fig. 1F, G). ERα target genes, progesterone receptor (PR) and cyclin D1 were unchanged between MCF7 and MCF7b cells (Fig. 1H, I) and nuclear ERα levels were similarly enhanced in response to estradiol (E2) treatment (Fig. 1J and Fig. S1D, E). To further investigate estrogen responsiveness, MCF7 and MCF7b cells were cultured in charcoal-stripped FBS-containing media supplemented with and without exogenous E2 and proliferation was monitored over 3 days. Both cell lines displayed enhanced proliferation with E2 supplementation (Fig. 1K; p=0.0236–0.0486) and unchanged viability regardless of E2 supplementation (Fig. 1L). Together, these results suggest that MCF7b cells exhibit similar

estrogen responsiveness to the parental line and that this signaling axis likely does not provide an enhanced E2-dependent or independent growth advantage to MCF7b cells.

MCF7b cells displayed a significant 2–3-fold increase in cell migration (Fig. 2A, B; p=0.0001–0.0026) and invasion (Fig. 2C, D; p=0.0982–0.0395) compared to the parental line. Additionally, cell adhesion was enhanced in MCF7b cells as indicated by a significant increase in crystal violet staining absorbance and area (Fig. 2E–G; p=0.0080–0.0425). Importantly, the number of cells per field was significantly increased (Fig. 2H; p=0.0356) while the area per cell remained unchanged (Fig. 2I), suggesting that adhesive ability rather than cell spreading is significantly augmented in MCF7b cells.

Next, we sought to investigate MCF7b enhanced metastatic potential *in vivo* and evaluate primary tumor establishment. To this end, parental MCF7 and MCF7b were re-inoculated into the mammary fat pad of mice with estradiol supplementation to enable robust tumor formation. Strikingly, MCF7b cells exhibited a significant reduction in primary tumor growth compared to the MCF7 line, which was confirmed by final tumor weight at the experimental endpoint (Fig. 3A–C; p=0.0079–0.0471). Upon sacrifice, primary tumors and hindlimbs were dissected and processed to assess tumor burden by flow cytometry, qPCR, microCT, or histology (Fig. S2A). MicroCT and histomorphometric analysis showed dramatic increases in bone volume as expected due to E2 supplementation, but did not reveal any significant differences in bone microarchitecture between MCF7- and MCF7b-inoculated mice (Fig. S2B–D).

Human-specific CD298 expression has been used to sensitively detect human tumor cells in the bone marrow of mice [29, 30] and was equivalently expressed in >99.9% of MCF7 and MCF7b cells *in vitro* (Fig. S2E). Flow cytometric analysis for CD298 expression in the bone marrow revealed a similar total number of CD298+ tumor cells between the two groups, but a significant increase in the percent of tumor cells in the bone marrow in MCF7b-inoculated mice (Fig. 3D; p=0.0196). Importantly, the percent tumor cells takes into account the total viable cells (bone marrow cells + tumor cells) per mouse, which varied slightly between mice but was not significantly different between groups (Fig. S2F), allowing for direct comparison of tumor burden between individual mice. Given the dramatic difference in primary tumor development, we normalized the CD298+ tumor cells to the final tumor weight to better assess metastatic potential, which revealed a dramatic increase in MCF7b dissemination to the bone (Fig. 3E; p=0.0003–0.0093).

Tumor burden as assessed by qPCR for the human housekeeping genes beta-2-microglobulin (*B2M*) and hypoxanthine phosphoribosyltransferase 1 (*HPRT1*) was modestly increased in whole femora (Fig. 3F and Fig. S2G; p=0.1540–0.6880) and significantly increased in spine homogenates in MCF7b-inoculated mice (Fig. 3G and Fig. S2H; p=0.0289–0.1643) (Table S1). In contrast, dissemination to the lung was reduced in the MCF7b-inoculated group, although this did not reach statistical significance (Fig. 3H and Fig. S2I; p=0.2345–0.2771) (Table S1).

Despite the enhanced tumor cell dissemination to the bone marrow of MCF7b-inoculated mice, it was unclear whether these results were due to enhanced dissemination from the

primary tumor site or increased bone homing. Thus, to distinguish between these processes and better understand the metastatic advantage of MCF7b cells, we inoculated MCF7 or MCF7b cells without exogenous estrogen supplementation by intracardiac inoculation (Fig. 3I), which recapitulates bone homing while bypassing tumor dissemination from the primary tumor. Radiographic analysis showed a modest increase in lesion number and lesion area in MCF7b-inoculated mice at weeks 18 and 22 post-tumor cell inoculation with extensive bone destruction occurring in a single tibia of two MCF7b-inoculated mice (Fig. 3J, K and Fig. S2K, L; p=0.0532–0.2428). Mice were sacrificed 22 weeks after tumor cell inoculation when the aforementioned two mice became paraplegic and moribund. To assess tumor burden in the bone, hindlimbs were dissected and processed for flow cytometry, qPCR, microCT or histology (Fig. S2J). No substantial differences were observed in bone microarchitecture by microCT (Fig. 3L, M and Fig. S2M) or tumor burden by flow cytometry (Fig. 3N and Fig. S2N) and qPCR analysis (Fig. 3O and Table S2). Although histomorphometric analysis of the tibiae also did not reveal any significant differences in bone volume between the groups (Fig. S2O), hematoxylin and eosin staining of tibiae confirmed substantial tumor burden in the bones of the two mice (mouse 11 and 15) that exhibited extensive osteolytic lesions by radiography (Fig. 3P, Q and Fig. S2P). The extent of tumor burden was particularly striking given the lack of exogenous estrogen in these mice. Immunostaining for pan-cytokeratin [31] confirmed the presence of tumor cells in these mice (Fig. 3Q and Fig. S2P), but did not detect tumor cells in any other MCF7b-inoculated mice or any of the MCF7-inoculated mice. Mice harboring overt MCF7b metastases (n=2) showed increased TRAP staining on the bone surface and had the highest osteoclast surface/bone surface (Oc.S/BS) and osteoclast number/bone perimeter (N.Oc/B.Pm) compared to other MCF7b-inoculated mice with no overt metastases or MCF7-inoculated mice (Fig. 3Q and Fig. S2Q). Collectively, these data suggest that the enhanced tumor burden in the skeleton following mammary fat pad inoculation of MCF7b cells is due to an increase in spontaneous dissemination from the primary tumor site to the skeleton, rather than enhanced bone colonization following intravasation. The MCF7b cells thus serve as a useful model to identify molecular factors that drive the process of spontaneous dissemination to the bone marrow.

Genomic and proteomic profiling identifies PREX1 as potential driver of the MCF7b phenotype

In order to identify mediators of tumor dissemination to the bone, we performed molecular profiling of parental MCF7 and MCF7b cells by reverse phase protein array (RPPA) and RNA sequencing (RNA-seq). RNA-seq analysis showed 3,685 genes were significantly altered (log2 fold-change > 1, $p<0.05$) and of the 296 total and phospho-specific antibodies that were tested by RPPA, twelve proteins were significantly altered in MCF7b cells (Fig. 4A, B; p=0.0002–0.0448). Further examination of these twelve genes in the RNA-seq dataset revealed three genes (*PREX1*, *HSPB1*, *DUSP4*) that were significantly altered in MCF7b cells by more than 2-fold (1 log2 fold-change by edgeR analysis with a significance of $p<0.05$) (Fig. 4C). Elevated *PREX1* and *HSPB1* expression in MCF7b cells compared to MCF7 or parental MCF7 (MCF7p) cells was validated by qPCR analysis (Fig. 4D, E; p=0.0112–0.0316). *DUSP4* was not significantly altered in MCF7b cells (Fig. 4F). Consistent with the expression pattern of these genes in MCF7b cells, analysis of all breast

cancer subtypes in The Cancer Genome Atlas (TCGA) provisional dataset revealed that PREX1 and HSPB1 were amplified/upregulated in 5–10% of breast cancer patients, whereas DUSP4 was deleted/down-regulated in ~9% of patients (Fig. 4G). Analysis of TCGA METABRIC dataset across all subtypes revealed similar genetic alterations for PREX1 and HSPB1 (Fig. 4H); however, DUSP4 was predominantly amplified/upregulated in this dataset. As previously reported using other breast cancer datasets [16, 22], PREX1 mRNA and protein expression was significantly higher in ER+ primary breast tumors compared to other subtypes in TCGA (Fig. 4I, J). We also confirmed a nearly two-fold increase in PREX1 protein levels in MCF7b cells compared to the parental line (Fig. 4K; p=0.0063). Together, these findings suggested an association of PREX1 upregulation with ER+ breast cancer, prompting us to pursue PREX1 as a mediator of the ER+ MCF7b metastatic phenotype.

PREX1 mediates MCF7b metastatic potential and skeletal dissemination

To investigate the contribution of PREX1 to the metastatic phenotype of MCF7b cells, we depleted PREX1 using either pooled siRNAs or two-independent shRNAs. Compared to the MCF7b non-silencing control line (NSC), RNAi-mediated knockdown resulted in PREX1 expression similar to that observed in MCF7 cells (Fig. S3A; p= 0.0005–0.0212). PREX1 knockdown blunted the increased migration (p=0.0445–0.3031) and almost completely reversed the invasive phenotype (p=0.0137–0.0376) of MCF7b cells (Fig. 5A–D). Similarly, knockdown of PREX1 modestly reduced the increased adhesive ability of MCF7b cells (Fig. 5E–H and Fig. S4A–D; p=0.1569–0.9313) and had no effect on the area per cell (Fig. 5I and Fig. S4E). Together, these results suggest that PREX1 mediates the enhanced invasive phenotype of MCF7b cells *in vitro*.

To determine whether PREX1 drives MCF7b dissemination from the primary tumor site, we transduced MCF7 or MCF7b cells with GIPZ lentiviral vectors containing GFP and either a NSC shRNA or PREX1-specific shRNA (shPREX1#1 or shPREX1#2; Fig. S3B). MCF7 NSC, MCF7b NSC, and MCF7b PREX1-knockdown lines exhibited similar cell proliferation (Fig. S3C), cell survival (Fig. S3D–F), and estrogen responsiveness (Fig. S3C, G, H). Additionally, PREX1 knockdown did not alter CD298 expression (Fig. S3I). MCF7 NSC, MCF7b NSC, or MCF7b PREX1-knockdown cells were inoculated into the mammary fat pad of mice supplemented with exogenous estradiol. As previously observed, MCF7b cells grew poorly at the primary tumor site as indicated by tumor volume (p=0.0001–0.0238) and final tumor weight (Fig. 6A–C; p=0.0022–0.0427). Upon sacrifice, primary tumors and hindlimbs were dissected and processed for flow cytometry, qPCR, or histology (Fig. S5A). Discernable primary tumors were identified in 9/10 (90%) MCF7 NSC-inoculated, 5/7 (71%) MCF7b NSC-inoculated, 8/10 (80%) MCF7b shPREX1#1-inoculated, and 2/7 (29%) MCF7b shPREX1#2-inoculated mice. Notably, PREX1 knockdown did not rescue primary tumor growth of MCF7b cells (Fig. 6A–C). Analysis of primary tumor homogenates by qPCR demonstrated that *PREX1* expression remained significantly upregulated in MCF7b NSC tumors and depleted in MCF7b PREX1-knockdown tumors (Fig. 6D; p=0.0026–0.0074). Flow cytometric analysis for GFP+ or CD298+ tumor cells revealed a significant increase in the number and percent of tumor cells in the bone marrow of MCF7b NSC-inoculated mice, which was diminished in both PREX1 knockdown cohorts (Fig. 6E;

p=0.0006–0.0425 and Fig. S5B). Given that primary tumors were not clearly discernable in several mice inoculated with MCF7b NSC (2/10 mice), MCF7b shPREX1#1 (2/10 mice) and MCF7b shPREX1#2 (5/7 mice) cells, these flow cytometry results were not normalized to primary tumor size as was performed in Figure 3E. Loss of PREX1 dramatically reduced the ability of MCF7b cells to disseminate to the femur (Fig. 6F and Fig. S5C; p=0.0021–0.0049) and spine (Fig. 6G and Fig. S5D; p=0.2426–0.4261) as assessed by qPCR for human housekeeping genes (Table S3). Consistent with our previous results, dissemination to the lung was reduced in MCF7b-inoculated mice and was not altered with PREX1 knockdown (Fig. 6H and Fig. S5E; p=0.2214–0.9968). Histomorphometric analysis did not reveal any discernable tumor cells or significant changes in bone volume in any of the groups (Fig. S5F, G).

Given our finding that PREX1 mediates tumor invasiveness and dissemination to the bone *in vivo*, we next sought to investigate the association of PREX1 expression with these clinicopathological characteristics in breast cancer patients. Analysis of two independent publically available datasets (GSE29044 and GSE14548) [32, 33] revealed that *PREX1* mRNA expression is significantly increased in ER+ invasive ductal carcinomas (IDC) compared to normal breast tissue (Fig. 6I, J; p=0.0001–0.0234). A separate breast cancer dataset including all molecular subtypes (81% ER+, 19% ER-) (GSE46141) [34] showed that in comparison to patients with local or lymph node dissemination, *PREX1* mRNA levels were significantly higher in the primary tumors of patients who developed distant metastases (Fig. 6K; p=0.0152–0.0388), as demonstrated by two PREX1 microarray probes. Interestingly, patients within the distant metastasis group that harbored bone metastases, indicated as red dots in Figure 6K, tended to express above average *PREX1* mRNA.

Discussion

The multi-step progression of the metastatic cascade is well established, but the mechanisms controlling tumor dissemination and colonization of distant organs, particularly the skeleton, remain less clear. Using a novel spontaneous model of bone metastasis derived from the human ER+ MCF7 line, the studies presented herein identify PREX1 as a mediator of tumor cell dissemination to skeletal sites. Loss of PREX1 diminishes the enhanced migration, invasion, and adhesion phenotype of bone-tropic MCF7 (MCF7b) cells *in vitro* and dissemination to bone from the primary tumor site *in vivo* (Fig. 6L). Clinically, PREX1 up-regulation frequently occurs in ER+ tumors and is associated with invasive breast cancer and distant metastasis. Together, our findings suggest that PREX1 is a clinically relevant mediator of invasion and dissemination of ER+ tumor cells to the skeleton, joining only a handful of molecules that have been identified to drive the spontaneous metastasis of breast cancer cells from the primary tumor site to the bone marrow.

PREX1 has been shown to promote metastasis to the lungs and lymph nodes in metastasis models of melanoma [19] and prostate cancer [20], respectively. Unfortunately, many published datasets investigating molecular changes associated with bone metastasis in breast cancer did not include PREX1 probes and thus the role of PREX1 cannot be gleaned from these analyses. However, recent molecular profiling data of human ER+ T47D cells that homed to the bone following intracardiac inoculation[35] showed a small but consistent

increase in PREX1 expression compared to parental cells (data not shown; n=2 mice/group, 1.1-fold, p=0.0903). In contrast, analysis of ER- human bone-metastatic MDA-MB-231 cells (GSE66495) exhibited decreased PREX1 expression compared to the parental line (data not shown; n=3 mice/group, 2.6-fold, p=0.0912). Studies performed in the ER- mouse 4T1 cell line yielded similar results with reduced PREX1 expression in tumor cells that had metastasized to the bone compared to the primary tumor [10]. Taken together, these data suggest that PREX1 may play dramatically different roles in the metastasis of ER+ versus ER- tumor cells.

Evaluation of PREX1 expression in breast cancer patient samples has also generated conflicting results, which may be a result of subtype-specific effects. Importantly, these studies have reported the association of PREX1 with metastasis across all subtypes of breast cancers and have not performed similar analyses for individual molecular subtypes. In support of our mechanistic findings, PREX1 levels were increased in primary breast and prostate tumors of patients who developed distant or lymph node metastases compared to those that did not harbor metastases[16, 19]. Additionally, a small cohort of 36 patients showed high PREX1 expression was associated with reduced disease-free survival[15]. In contrast, PREX1 expression was associated with improved patient outcome in a study of 2000 breast cancer patients representing all molecular subtypes[23]. Overall survival in patients harboring PREX1 genetic alterations or those specifically harboring amplification/upregulation of PREX1 across all subtypes was not significantly changed in the two datasets we investigated using cBioPortal for Cancer Genomics (data not shown). Using immunohistochemistry, Marotti et al. reported similar PREX1 levels between patients with and without metastases as well as between matched primary tumors and metastases across all molecular subtypes [22]. PREX1 levels were modestly decreased in bone metastases compared to visceral metastases (106 ± 61 versus 156 ± 69, p=0.008); however, expression varied greatly between patients, independent of tumor subtype, making it difficult to interpret PREX1 expression in site-specific metastasis. While this study reported PREX1 levels in the primary tumor and metastases for each molecular subtype, analyses were performed without subtype separation likely as a consequence of the small sample size (~50 patients).

Previous reports suggest that PREX1 activation of downstream Rac signaling is responsible for enhanced metastatic potential of melanoma and prostate cancer cells[16, 19, 20]; however, this possibility has not been extensively investigated *in vivo*. Molecular profiling of MCF7b and parental cells did not reveal any changes in Rac signaling (Rac, PAKs, mTOR, etc) suggesting this may not be the prominent mechanism by which PREX1 promotes MCF7b dissemination. It also remains unclear why PREX1 upregulation preferentially promotes dissemination to bone over other sites in the MCF7b model. Previous work indicates that PREX1 is activated by CXCR4 [16, 36], a well-known chemokine receptor involved in tumor cell homing to the bone. However, CXCR4 mRNA expression was similar between MCF7 and MCF7b cells by RNA-seq (data not shown).

Strikingly, MCF7b cells grew poorly following re-inoculation in the primary tumor site despite having enhanced PREX1 mRNA expression at the experimental endpoint and efficiently disseminating to the bone in two independent experiments. These data are in

support of previously published work showing that PREX1 overexpression did not alter primary tumor growth in a prostate cancer xenograft model, but did enhance dissemination of tumor cells to the lymph nodes[21]. However, several reports indicate that loss of PREX1 reduces primary tumor growth in ER+ models[15–17]. Given that PREX1 knockdown did not rescue MCF7b primary tumor growth, our data suggests that the mechanisms mediating poor tumor growth following MCF7b re-inoculation into the orthotopic site are independent of PREX1.

The contribution of PREX1 to tumor cell proliferation also remains controversial. Several groups have shown that PREX1 does not affect *in vitro* proliferation or activation of ERK signaling in breast[37], melanoma[38], or glioblastoma cancer cells[39]. However, others implicate PREX1 in activating IGF-1R/InsR[15], PI3K/AKT[17], and MEK/ERK[17, 18] signaling following growth factor stimulation *in vitro* and that this signaling activation promotes primary tumor growth *in vivo*[16, 17]. These findings suggest that tumor-inhibitory mechanisms may be increased in MCF7b cells, limiting primary tumor establishment, or that MCF7b cells have become molecularly primed to grow in the bone rather than the orthotopic site. Despite the enrichment of tumor cells in the bone marrow of MCF7b mammary fat pad-inoculated mice, overt bone metastases did not develop during the 8-week experimental timeline. These results are not surprising given the known low metastatic potential of the MCF7 cell line and relatively short timeline for the experiment, which had to be stopped due to estradiol-related toxicities. This is further supported by the long latency period (22 weeks) observed in the intracardiac study, which lacked exogenous estradiol, but had to be stopped due to the moribund state of the two mice who developed overt tumors in the bone. Given these timelines, it remains unknown whether all spontaneously disseminated MCF7b cells would eventually progress into overt metastases if provided a more extended time course.

Intracardiac inoculation of MCF7b cells resulted in overt bone metastases in 20% of mice (2/10 mice), compared with 0% in the MCF7-bearing mice, in the absence of exogenous estradiol. Interestingly, the development of overt bone metastases in a small fraction of mice has been observed in similar studies using the ER+ bone metastatic derivatives of MCF7 (MCF7–5624A[40]) and T47D (DBM[35]) cells. With the exception of the two MCF7b-inoculated mice with overt metastases, tumor burden was very similar between MCF7-inoculated and MCF7b-inoculated mice. These results suggest that PREX1 upregulation or other molecular alterations harbored by MCF7b cells may not drive spontaneous progression and outgrowth of bone-disseminated tumor cells into overt bone metastases, but rather prime MCF7b cells to leave the primary tumor site; however, it is notable that lesion area approached significance in the intracardiac-inoculated model (Fig. 3J). For this reason, we cannot entirely rule out the possibility that PREX1 or other molecular alterations harbored by the MCF7b cells mediates metastatic progression and outgrowth in bone. Since 20% of MCF7b intracardiac-inoculated mice developed overt bone metastases, it is possible that the bone-disseminated MCF7b cells are more sensitive to microenvironmental stimuli that trigger metastatic outgrowth or that they secrete factors that initiate tumor-induced bone destruction. For example, immunostaining following intracardiac inoculation of MCF7 and MCF7b cells revealed an increase in TRAP+ osteoclasts lining the bone surface in tibiae harboring overt MCF7b metastases compared to MCF7b-inoculated mice with no overt

metastases and control MCF7-inoculated mice, suggesting tumor-induced expansion of the osteoclast population. The vicious cycle of bone destruction is a well-described process that disrupts physiological bone remodeling, resulting in enhanced osteoclastogenesis, resorption of bone matrix, and localized release of growth factors and cytokines that promote tumor cell proliferation [4]. However, PTHrP and GLI2 expression and basal ERK, AKT, or SMAD signaling, which are known to be activated by bone-derived growth factors such as TGFβ and IGFs and promote tumor-induced bone destruction [41–43], were unchanged between the MCF7b and parental cell line *in vitro* (Fig. 1I and data not shown). These data suggest that these well-known mechanisms of tumor-induced bone disease likely did not trigger the outgrowth of these cells. Thus, the MCF7b model may also serve as a physiologically relevant model for future studies to identify other factors mediating metastatic outgrowth.

In summary, PREX1 drives preferential dissemination of tumor cells from the primary tumor site to the bone in a human ER+ model of spontaneous metastasis. Knockdown of PREX1 in bone-tropic MCF7 cells diminishes the enhanced metastatic potential *in vitro* and *in vivo* and is consistent with elevated PREX1 levels in ER+ breast cancer patients being associated with invasive disease and distant metastasis. These findings provide a mechanism by which tumor cells spontaneously disseminate from the primary tumor site to the bone marrow and a physiologically relevant model for further investigation of tumor dissemination and metastatic outgrowth.

Materials and Methods

Cell lines

Cells—Human parental MCF7 (MCF7p) breast cancer cells were obtained from ATCC and transduced with a lentiviral vector containing GFP and a non-silencing (NSC) short hairpin (Dharmacon) to generate MCF7-NSC (MCF7) cells. Bone-selective MCF7 (MCF7b) cells were isolated from the bone marrow approximately 6 months following implantation of MCF7 cells into the mammary fat pad. All cell lines were cultured as previously described[31] and were recently re-authenticated by ATCC. All cell lines have been recently tested for mycoplasma and found to be negative.

siRNA and shRNA—Knockdown experiments were performed as previously described [44]. See the Supplementary Materials and Methods section for detailed experimental procedures.

Proliferation assays

For trypan blue exclusion assays, cells were trypsinized and mixed with trypan blue solution. Viable cells were determined based on dye exclusion and were counted using a TC20 Automated Cell Counter (Bio-Rad). CellTrace Violet proliferation assays were performed by staining cells with CellTrace Violet dye (Thermo Fisher) according to the manufacturer's instructions and culturing cells for a total of seven days. A portion of cells were fixed with 10% formalin for 20 minutes on days 4, 7, and 10, washed with PBS, and stored in PBS at 4°C until analysis. CellTrace Violet fluorescence intensity was analyzed in

the VUMC Flow Cytometry Shared Resource using the 5-laser BD LSRII. Datasets were analyzed using FlowJo software (FlowJo, LLC). For E2-dependent proliferation assays, cells were grown in charcoal-stripped FBS-containing (cs-FBS) media (Millipore Sigma, Catalog No. F6765) for 1.5 weeks prior to initiation of experiments to ensure estrogen deprivation. Cells were cultured in cs-FBS media in the presence or absence of E2 (10nM; Millipore Sigma, Catalog No. E2758) for a total of 3 days. Each day, proliferation and viability was assessed by trypan blue exclusion.

Annexin V/PI/Hoechst Staining

Viability was assessed on day 3 of E2-dependent proliferation assays by staining cells with Annexin V (Thermo, Catalog No. A35110) according to the manufacturer's instructions. Following Annexin V staining, cells were washed and resuspended in 1% BSA in PBS and Hoechst 33342 (1μg/ml; ThermoFisher, Catalog No. H3570) or PI (25ng; BD Pharmingen, Catalog No. 556463) to mark dead cells. Flow cytometry experiments were analyzed in the VMC Flow Cytometry Shared Resource using the 5-laser BD LSRII. Datasets were analyzed using FlowJo software (FlowJo, LLC).

Western blotting

Protein expression was assessed as previously described [44]. See the Supplementary Materials and Methods section for detailed experimental procedures.

Migration and invasion assays

Cells were seeded at 1×10^5 cells per well into 24-well transwell inserts with 8μm pores (Corning). For invasion assays, transwell inserts were coated with 0.5mg/ml matrigel for 30 minutes at 37°C prior to cell seeding. Serum-free medium was added to the upper chamber and medium containing 1% FBS was added to the bottom chamber to create a chemoattractant gradient. Cells were incubated on plates for 72 hours and fixed/permeabilized with methanol for 10 minutes. Transwell inserts were stained with 0.5% crystal violet for 10 minutes, washed with water, and allowed to dry overnight. Bright-field images were acquired using an inverted microscope. The transwell membrane was removed from the insert and mounted onto coverslips using VECTASHIELD HardSet Antifade Mounting Medium with DAPI (Vector Laboratories). Images were collected on an Olympus BX41 Microscope equipped with an Olympus DP71 camera using the 10X and 40X plan objectives and quantified using ImageJ software.

Adhesion assays

5μg/ml or 10 μg/ml fibronectin (Thermo Fisher) was incubated on a 96-well plate for 1 hour at room temperature. Wells were washed twice with PBS and allowed to dry. Cells were seeded at 0.5×10^5 in 100μl of serum-free medium per well and incubated for 30 minutes or 1 hour. Following incubation, the medium was removed and wells gently washed with PBS. Cells were fixed/permeabilized in methanol for 10 minutes, stained with 0.5% crystal violet for 10 minutes, washed with water, and allowed to dry. Bright-field images were collected on an inverted microscope using the 10X plan objective and analyzed using ImageJ software. For absorbance measurements, 100μl of 30% acetic acid in PBS was added per

well and incubated with rotation for 10 minutes. The absorbance was read at 600nm using a GloMax Discover microplate reader (Promega Corp).

Reverse Phase Protein Array (RPPA)

Cells were seeded at 2×10^6 cells per well in a 6-well plate and cultured overnight. Cells were washed twice with PBS and 100μl of RIPA buffer was added to each well and incubated for 20 minutes at 4°C. Protein concentration was determined by BCA, adjusted to 1.5μg/μl, and mixed with sample buffer (4X SDS and beta-mercaptoethanol). Samples were boiled for 5 minutes and stored at −80°C until sent to MD Anderson Cancer Center. RPPA was performed, processed, and analyzed by the RPPA Core facility at MD Anderson Cancer Center (Table S4).

RNA-sequencing and bioinformatics

RNA samples for MCF7 and MCF7b cells (n= 3 independent replicates/group) were sequenced by the Stanford Functional Genomics Facility and analyzed by the VANGARD core at Vanderbilt University Medical Center as previously described [45]. Log2 fold change values were computed using the EdgeR package. These data have been deposited in the GEO database under accession number GSE121677.

Real-time qPCR

Cells were harvested and analyzed by real-time qPCR as previously described [44]. Whole femur homogenates and real-time qPCR analysis was performed as previously described [31]. See the Supplementary Materials and Methods section for detailed experimental procedures.

In silico analyses

TCGA patient data analysis—The cBioPortal for Cancer Genomics was accessed on 10 September 2018 to determine PREX1 genetic alterations in all breast cancer subtypes using the TCGA provisional dataset and the METABRIC, Nature 2012, & Nat Commun 2016 dataset [46, 47]. PREX1 expression from the first dataset was downloaded and entered into Prism to determine statistical differences between breast cancer subtypes. *GSE14548* (Ma et al., 2009) and *GSE29044 (Colak et al., 2013) datasets*. The data were queried for PREX1 expression (Hs.109315.1.S1_3p_a_at and 224909_s_at) and samples were separated into normal, ductal carcinoma in situ (DCIS), or ER+ invasive ductal carcinoma (IDC). *GSE46141 (Kimbung et al, Mol Oncol) dataset.* The ER+ patient data were queried for PREX1 expression (100308105_TGI_at and 100152751_TGI_at) and patients were separated into local-regional relapse (skin, breast), lymph node metastasis, or distant metastasis (liver, bone, lung).

Animals

All experiments were performed following the relevant guidelines and regulations of the Animal Welfare Act and the Guide for the Care and Use of Laboratory Animals and were approved by the Institutional Animal Care and Use Committee (IACUC) at Vanderbilt University. All experiments were performed using 4–6 week old female athymic nude mice

(Jackson, Cat #7850). For orthotopic inoculation studies, sample size was determined using PS: Power and Sample Size Calculation software developed by Vanderbilt University. 17β-estradiol pellets (0.5 mg, 60-day release, Innovative Research of America) were implanted subcutaneously into female athymic nude mice. The next day, 5×10^5 tumor cells in 20μl volume of sterile PBS+50% matrigel (Fisher Scientific) were injected into the fourth mammary fat pad (n=10 mice/group). Tumor volume was assessed by caliper measurement. Several mice were found dead or had to be sacrificed early due to estrogen toxicities and therefore were removed from the final analysis. For the original primary tumor study, the final analysis included 8/10 MCF7-inoculated mice and 8/10 MCF7b-inoculated mice. For the PREX1 knockdown primary tumor study, the final analysis included 10/10 MCF7 NSC-inoculated, 7/10 MCF7b NSC-inoculated, 10/10 MCF7b shPREX1#1-inoculated, and 7/10 MCF7b shPREX1#2-inoculated mice. For intracardiac inoculation, power calculations were performed by Rie von Eyben, a radiation oncology statistician at Stanford University. For the intracardiac study, female athymic nude mice were inoculated with 1×10^5 tumor cells in the absence of 17β-estradiol pellets as previously described [44, 48] (n=10 mice/group). One mouse was found dead at 15 weeks and the remaining mice were euthanized at 22 weeks post-tumor cell inoculation. The final analysis included 9/10 MCF7-inoculated and 10/10 MCF7b-inoculated mice. The mouse experiments were not randomized. The investigator was blinded for radiographic and histological analysis.

Radiography

Radiographic (x-ray) images were obtained as previously described [49]. Briefly, a Faxitron LX-60 (34kV for 8 seconds) was used to acquire x-ray images. Using ImageJ software, each osteolytic lesion (defined as a region of reduced bone density) was counted, outlined and the outlined area measured (Figure S2L). The total “lesion area per mouse” was calculated as the sum of the areas of all lesions. Similarly, the total “lesion number per mouse” was determined by totaling the number of osteolytic lesions.

Microcomputed tomography (microCT)

Ex vivo microCT (Scanco50) was performed as previously described [31]. See the Supplementary Materials and Methods section for detailed experimental procedures.

Flow cytometry

Samples were isolated and analyzed by flow cytometry as previously reported [31]. Briefly, hindlimbs were flushed using centrifugation to isolate bone marrow and red blood cells were lysed. Bone marrow cells (1×10^6) cells or cultured tumor cells were stained with CD298 (BioLegend, Cat #341704, 175ng) for 30 minutes on ice in the dark. Analysis was performed in the VUMC Flow Cytometry Shared Resource using the 5-laser BD LSRII and data were analyzed using FlowJo software (FlowJo, LLC).

Immunostaining

Pan-cytokeratin staining was performed on tibiae as previously described [31]. See the Supplementary Materials and Methods section for detailed experimental procedures including ERα and TRAP staining.

Statistical methods

For all studies, *n* per group is as indicated in the figure legend and the scatter dot plots indicate the mean of each group and the standard error of the mean. All graphs and statistical analyses were generated using Prism software (Graphpad). All *in vitro* and *in vivo* assays were analyzed for statistical significance using Mann-Whitney test, One-way ANOVA with Sidak's post-test, or Two-way ANOVA with Tukey's multiple comparisons test. See figure legends for detailed statistical analyses for each experiment. All *in vitro* experiments represent three biological replicates collected from independent experiments and no statistical method was used to predetermine sample size. Animal studies were performed once and included appropriate sample sizes for statistical evaluation. For all analyses, $P<0.05$ was statistically significant and *$P<0.05$, **$P<0.01$, ***$P<0.001$, ****$P<0.0001$.

Supplementary Material

Refer to Web version on PubMed Central for supplementary material.

Acknowledgements

The authors wish to acknowledge Mr. Joshua Johnson for histological processing and sectioning of tibiae. Flow Cytometry experiments were performed in the VMC Flow Cytometry Shared Resource, which is supported by the Vanderbilt Ingram Cancer Center (P30 CA68485) and the Vanderbilt Digestive Disease Research Center (DK058404). The authors wish to acknowledge the expert technical support of the VANGARD core facilities. RPPA data were generated by the RPPA Core facility at MD Anderson Cancer Center (NCI #CA16672). RWJ and MEC are supported in part by and funding for experiments was provided by NIH award R00CA194198 (RWJ). Experiments performed at Vanderbilt were supported in part by scholarship funds from NIH award P30CA068485 Vanderbilt-Ingram Cancer Center Support Grant.

References

1. Early Breast Cancer Trialists' Collaborative G. Comparisons between different polychemotherapy regimens for early breast cancer: meta-analyses of long-term outcome among 100 000 women in 123 randomised trials. Lancet. 2012;379(9814):432–44. [PubMed: 22152853]
2. Coleman RE. Clinical features of metastatic bone disease and risk of skeletal morbidity. Clin Cancer Res. 2006;12(20 Pt 2):6243s–9s. [PubMed: 17062708]
3. Weilbaecher KN, Guise TA, McCauley LK. Cancer to bone: a fatal attraction. Nat Rev Cancer. 2011;11(6):411–25. [PubMed: 21593787]
4. Johnson RW, Schipani E, Giaccia AJ. HIF targets in bone remodeling and metastatic disease. Pharmacol Ther. 2015;150:169–77. [PubMed: 25681658]
5. Coleman RE. Metastatic bone disease: clinical features, pathophysiology and treatment strategies. Cancer Treat Rev. 2001;27(3):165–76. [PubMed: 11417967]
6. Schröder J, Fietz T, Köhler A, Petersen V, Tesch H, Spring L, et al. Treatment and pattern of bone metastases in 1094 patients with advanced breast cancer – Results from the prospective German Tumour Registry Breast Cancer cohort study. European Journal of Cancer. 2017;79:139–48. [PubMed: 28494404]
7. Han HH, Lee SH, Kim BG, Lee JH, Kang S, Cho NH. Estrogen Receptor Status Predicts Late-Onset Skeletal Recurrence in Breast Cancer Patients. Medicine (Baltimore). 2016;95(8):e2909. [PubMed: 26937933]
8. Savci-Heijink CD, Halfwerk H, Hooijer GK, Horlings HM, Wesseling J, van de Vijver MJ. Retrospective analysis of metastatic behaviour of breast cancer subtypes. Breast Cancer Res Treat. 2015;150(3):547–57. [PubMed: 25820592]
9. Zhang XH, Wang Q, Gerald W, Hudis CA, Norton L, Smid M, et al. Latent bone metastasis in breast cancer tied to Src-dependent survival signals. Cancer Cell. 2009;16(1):67–78. [PubMed: 19573813]

10. Bidwell BN, Slaney CY, Withana NP, Forster S, Cao Y, Loi S, et al. Silencing of Irf7 pathways in breast cancer cells promotes bone metastasis through immune escape. Nat Med. 2012;18(8):1224–31. [PubMed: 22820642]
11. Kang Y, Siegel PM, Shu W, Drobnjak M, Kakonen SM, Cordón-Cardo C, et al. A multigenic program mediating breast cancer metastasis to bone. Cancer Cell. 2003;3(6):537–49. [PubMed: 12842083]
12. Lawson CD, Ridley AJ. Rho GTPase signaling complexes in cell migration and invasion. The Journal of Cell Biology. 2018;217(2):447–57. [PubMed: 29233866]
13. Porter AP, Papaioannou A, Malliri A. Deregulation of Rho GTPases in cancer. Small GTPases. 2016;7(3):123–38. [PubMed: 27104658]
14. Kazanietz MG, Caloca MJ. The Rac GTPase in Cancer: From Old Concepts to New Paradigms. Cancer research. 2017;77(20):5445–51. [PubMed: 28807941]
15. Montero JC, Seoane S, Ocaña A, Pandiella A. P-Rex1 participates in Neuregulin-ErbB signal transduction and its expression correlates with patient outcome in breast cancer. Oncogene. 2010;30:1059. [PubMed: 21042280]
16. Sosa MS, Lopez-Haber C, Yang C, Wang H, Lemmon MA, Busillo JM, et al. Identification of the Rac-GEF P-REX1 as an essential mediator of ErbB signaling in breast cancer. Molecular cell. 2010;40(6):877–92. [PubMed: 21172654]
17. Dillon LM, Bean JR, Yang W, Shee K, Symonds LK, Balko JM, et al. P-REX1 creates a positive feedback loop to activate growth factor receptor, PI3K/AKT, and MEK/ERK signaling in breast cancer. Oncogene. 2015;34(30):3968–76. [PubMed: 25284585]
18. Liu H-J, Ooms LM, Srijakotre N, Man J, Vieusseux J, Waters JE, et al. PtdIns(3,4,5)P(3)-dependent Rac Exchanger 1 (PREX1) Rac-Guanine Nucleotide Exchange Factor (GEF) Activity Promotes Breast Cancer Cell Proliferation and Tumor Growth via Activation of Extracellular Signal-regulated Kinase 1/2 (ERK1/2) Signaling. The Journal of Biological Chemistry. 2016;291(33):17258–70. [PubMed: 27358402]
19. Lindsay CR, Lawn S, Campbell AD, Faller WJ, Rambow F, Mort RL, et al. P-Rex1 is required for efficient melanoblast migration and melanoma metastasis. Nature Communications. 2011;2:555.
20. Qin J, Xie Y, Wang B, Hoshino M, Wolff DW, Zhao J, et al. Upregulation of PIP3-dependent Rac exchanger 1 (P-Rex1) promotes prostate cancer metastasis. Oncogene. 2009;28:1853. [PubMed: 19305425]
21. Qin J, Xie Y, Wang B, Hoshino M, Wolff DW, Zhao J, et al. Upregulation of PIP3-Dependent Rac Exchanger 1 (P-Rex1) Promotes Prostate Cancer Metastasis. Oncogene. 2009;28(16):1853–63. [PubMed: 19305425]
22. Marotti JD, Muller KE, Tafe LJ, Demidenko E, Miller TW. P-Rex1 Expression in Invasive Breast Cancer in relation to Receptor Status and Distant Metastatic Site. International Journal of Breast Cancer. 2017;2017:4537532. [PubMed: 28698809]
23. Cheng W-Y, Yang T-HO, Anastassiou D. Development of a Prognostic Model for Breast Cancer Survival in an Open Challenge Environment. Science Translational Medicine. 2013;5(181): 181ra50–ra50.
24. Barkan D, Kleinman H, Simmons JL, Asmussen H, Kamaraju AK, Hoenorhoff MJ, et al. Inhibition of metastatic outgrowth from single dormant tumor cells by targeting the cytoskeleton. Cancer Res. 2008;68(15):6241–50. [PubMed: 18676848]
25. Gustafsson KL, Farman H, Henning P, Lionikaite V, Moverare-Skrtic S, Wu J, et al. The role of membrane ERalpha signaling in bone and other major estrogen responsive tissues. Sci Rep. 2016;6:29473. [PubMed: 27388455]
26. La Rosa P, Pesiri V, Leclercq G, Marino M, Acconcia F. Palmitoylation regulates 17β-estradiol-induced estrogen receptor-α degradation and transcriptional activity. Mol Endocrinol. 2012;26(5): 762–74. [PubMed: 22446104]
27. Duplessis TT, Williams CC, Hill SM, Rowan BG. Phosphorylation of Estrogen Receptor α at serine 118 directs recruitment of promoter complexes and gene-specific transcription. Endocrinology. 2011;152(6):2517–26. [PubMed: 21505052]

28. Ali S, Metzger D, Bornert JM, Chambon P. Modulation of transcriptional activation by ligand-dependent phosphorylation of the human oestrogen receptor A/B region. EMBO J. 1993;12(3): 1153–60. [PubMed: 8458328]
29. Sowder ME, Johnson RW. Enrichment and detection of bone disseminated tumor cells in models of low tumor burden. Scientific Reports. 2018;8(1):14299. [PubMed: 30250146]
30. Lawson DA, Bhakta NR, Kessenbrock K, Prummel KD, Yu Y, Takai K, et al. Single-cell analysis reveals a stem-cell program in human metastatic breast cancer cells. Nature. 2015;526(7571):131–5. [PubMed: 26416748]
31. Sowder ME, Johnson RW. Enrichment and detection of bone disseminated tumor cells in models of low tumor burden. Scientific Reports. 2018;8:14299. [PubMed: 30250146]
32. Colak D, Nofal A, Albakheet A, Nirmal M, Jeprel H, Eldali A, et al. Age-specific gene expression signatures for breast tumors and cross-species conserved potential cancer progression markers in young women. PloS one. 2013;8(5):e63204–e. [PubMed: 23704896]
33. Ma X-J, Dahiya S, Richardson E, Erlander M, Sgroi DC. Gene expression profiling of the tumor microenvironment during breast cancer progression. Breast cancer research : BCR. 2009;11(1):R7–R. [PubMed: 19187537]
34. Kimbung S, Kovács A, Bendahl P-O, Malmström P, Fernö M, Hatschek T, et al. Claudin-2 is an independent negative prognostic factor in breast cancer and specifically predicts early liver recurrences. Molecular oncology. 2014;8(1):119–28. [PubMed: 24287398]
35. Gawrzak S, Rinaldi L, Gregorio S, Arenas EJ, Salvador F, Urosevic J, et al. MSK1 regulates luminal cell differentiation and metastatic dormancy in ER+ breast cancer. Nat Cell Biol. 2018;20(2):211–21. [PubMed: 29358704]
36. Kremer KN, Dinkel BA, Sterner RM, Osborne DG, Jevremovic D, Hedin KE. TCR-CXCR4 signaling stabilizes cytokine mRNA transcripts via a PREX1-Rac1 pathway: implications for CTCL. Blood. 2017;130(8):982–94. [PubMed: 28694325]
37. Barrio-Real L, Lopez-Haber C, Casado-Medrano V, Goglia AG, Toettcher JE, Caloca MJ, et al. P-Rex1 is dispensable for Erk activation and mitogenesis in breast cancer. Oncotarget. 2018;9(47): 28612–24. [PubMed: 29983884]
38. Ryan MB, Finn AJ, Pedone KH, Thomas NE, Der CJ, Cox AD. ERK/MAPK Signaling Drives Overexpression of the Rac-GEF, PREX1, in BRAF- and NRAS-mutant Melanoma. Molecular cancer research : MCR. 2016;14(10):1009–18. [PubMed: 27418645]
39. Gont A, Daneshmand M, Woulfe J, Lavictoire SJ, Lorimer IAJ. PREX1 integrates G protein-coupled receptor and phosphoinositide 3-kinase signaling to promote glioblastoma invasion. Oncotarget. 2017;8(5):8559–73. [PubMed: 28051998]
40. Ganapathy V, Banach-Petrosky W, Xie W, Kareddula A, Nienhuis H, Miles G, et al. Luminal breast cancer metastasis is dependent on estrogen signaling. Clinical & experimental metastasis. 2012;29(5):10.1007/s10585-012-9466-4.
41. Guo X, Wang X-F. Signaling cross-talk between TGF-β/BMP and other pathways. Cell research. 2009;19(1):71–88. [PubMed: 19002158]
42. Neuzillet C, Tijeras-Raballand A, Cohen R, Cros J, Faivre S, Raymond E, et al. Targeting the TGFβ pathway for cancer therapy. Pharmacology & Therapeutics. 2015;147:22–31. [PubMed: 25444759]
43. Rahman MS, Akhtar N, Jamil HM, Banik RS, Asaduzzaman SM. TGF-β/BMP signaling and other molecular events: regulation of osteoblastogenesis and bone formation. Bone Research. 2015;3:15005. [PubMed: 26273537]
44. Johnson RW, Finger EC, Olcina MM, Vilalta M, Aguilera T, Miao Y, et al. Induction of LIFR confers a dormancy phenotype in breast cancer cells disseminated to the bone marrow. Nat Cell Biol. 2016;18(10):1078–89. [PubMed: 27642788]
45. Johnson RW, Sun Y, Ho PWM, Chan ASM, Johnson JA, Pavlos NJ, et al. Parathyroid Hormone-Related Protein Negatively Regulates Tumor Cell Dormancy Genes in a PTHR1/Cyclic AMP-Independent Manner. Frontiers in Endocrinology. 2018;9:241. [PubMed: 29867773]
46. Cerami E, Gao J, Dogrusoz U, Gross BE, Sumer SO, Aksoy BA, et al. The cBio Cancer Genomics Portal: An Open Platform for Exploring Multidimensional Cancer Genomics Data. Cancer Discovery. 2012;2(5):401–4. [PubMed: 22588877]

47. Gao J, Aksoy BA, Dogrusoz U, Dresdner G, Gross B, Sumer SO, et al. Integrative Analysis of Complex Cancer Genomics and Clinical Profiles Using the cBioPortal. Science signaling. 2013;6(269):pl1–pl. [PubMed: 23550210]

48. Thomas RJ, Guise TA, Yin JJ, Elliott J, Horwood NJ, Martin TJ, et al. Breast Cancer Cells Interact with Osteoblasts to Support Osteoclast Formation. Endocrinology. 1999;140(10):4451–8. [PubMed: 10499498]

49. Johnson RW, Nguyen MP, Padalecki SS, Grubbs BG, Merkel AR, Oyajobi BO, et al. TGF-beta promotion of Gli2-induced expression of parathyroid hormone-related protein, an important osteolytic factor in bone metastasis, is independent of canonical Hedgehog signaling. Cancer Res. 2011;71(3):822–31. [PubMed: 21189326]

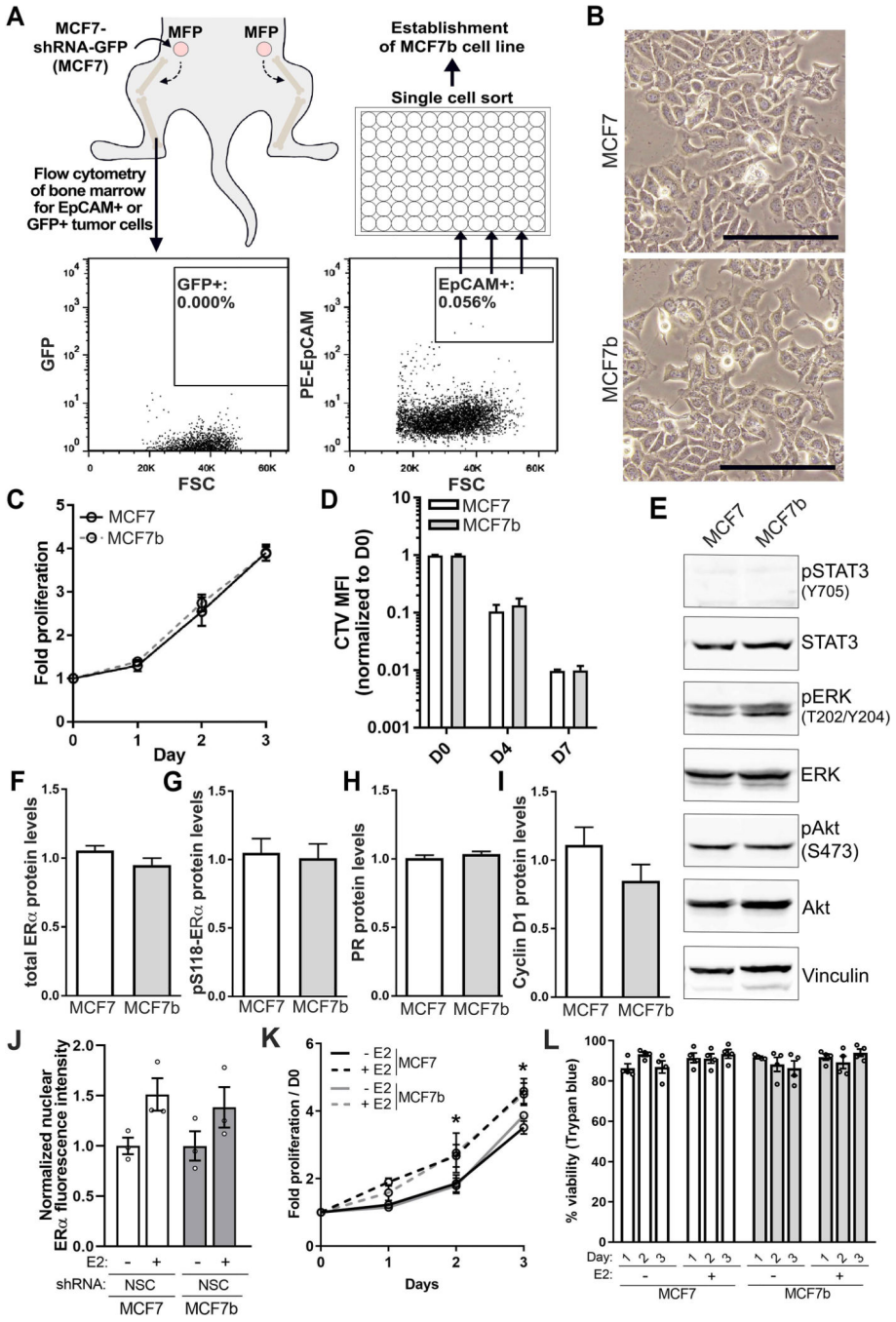

Figure 1. Establishment and characterization of the bone-metastatic MCF7 (MCF7b) model.

(A) MCF7-shRNA-GFP (MCF7) cells were injected into the mammary fat pad of nude mice (n=4) in the absence of exogenous estradiol and bone marrow was analyzed for EpCAM and GFP by flow cytometry approximately 6 months after tumor injection. EpCAM+ cells were sorted as single cells into a 96-well plate and the MCF7b line was established from one of the recovered clones. (B) Representative DIC images of MCF7 and MCF7b cell morphology following *in vitro* culture. All panels = 10X, scale bars = 200μm. (C) Trypan blue exclusion assay to assess fold change proliferation in MCF7 and MCF7b cells over 3 days. (D) MCF7

and MCF7b cells were dyed with CellTrace Violet proliferation dye and mean fluorescence intensity (MFI) was tracked over seven days to assess proliferation. (E) Representative western blot for pSTAT3-Y705, total STAT3, ERK-pT202/Y204, total ERK, pAKT-pS473, total AKT, and vinculin in MCF7 and MCF7b cells. (F-I) Normalized linear protein expression from RPPA analysis of (F) total ERα, (G) p118 ERα, (H) progesterone receptor (PR), and (I) cyclin D1 in MCF7 and MCF7b cells. (J) Normalized nuclear ERα fluorescence intensity in MCF7 and MCF7b cells grown in charcoal-stripped FBS-containing media with and without 17β-estradiol (E2) supplementation. (K) Trypan blue exclusion assay to assess fold change proliferation in MCF7 and MCF7b cells over 3 days grown in charcoal-stripped FBS-containing media with and without E2 supplementation. (L) Cell viability as assessed by trypan blue exclusion of cells described in (K). K: One-way ANOVA with Sidak's multiple comparisons test. *$p<0.05$. C-L: n= three independent biological replicates. Bar graphs indicate mean + standard error of the mean.

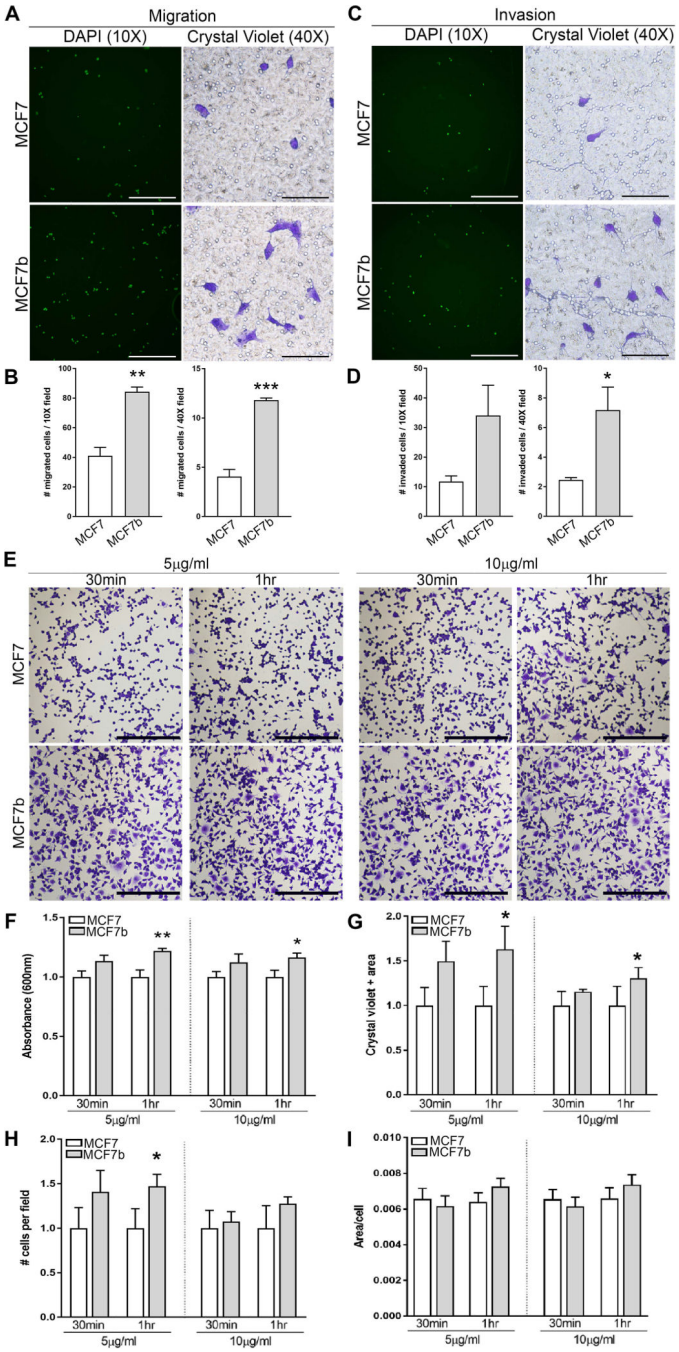

Figure 2. Invasive properties are increased in MCF7b cells.

(A) Representative images of MCF7 and MCF7b cell migration assessed by DAPI (green pseudocolor) or crystal violet staining. Left panel = 10X, scale bar = 500μm; right panel = 40X, scale bar = 100μm. (B) Quantitation of the number of migrated cells per 10X or 40X field from (A). (C) Representative images of cell invasion assessed as in (A). (D) Quantitation of the number of invaded cells per 10X or 40X field from (C). (E) Representative images of MCF7 and MCF7b cells incubated on 5μg/ml or 10μg/ml fibronectin for 30 minutes or 1 hour. All panels = 10X, scale bar = 500μm. (F) Crystal Violet

absorbance measurements at 600nm to assess adherent cells from (A). (G-I) Quantitation of (G) total crystal violet area per field, (H) number of cells per field, and (I) area per cell from (E). B, D, F-I: Mann-Whitney test. *p<0.05, **p<0.01, ***p<0.001. A-I: n= three independent biological replicates. Bar graphs indicate mean + standard error of the mean.

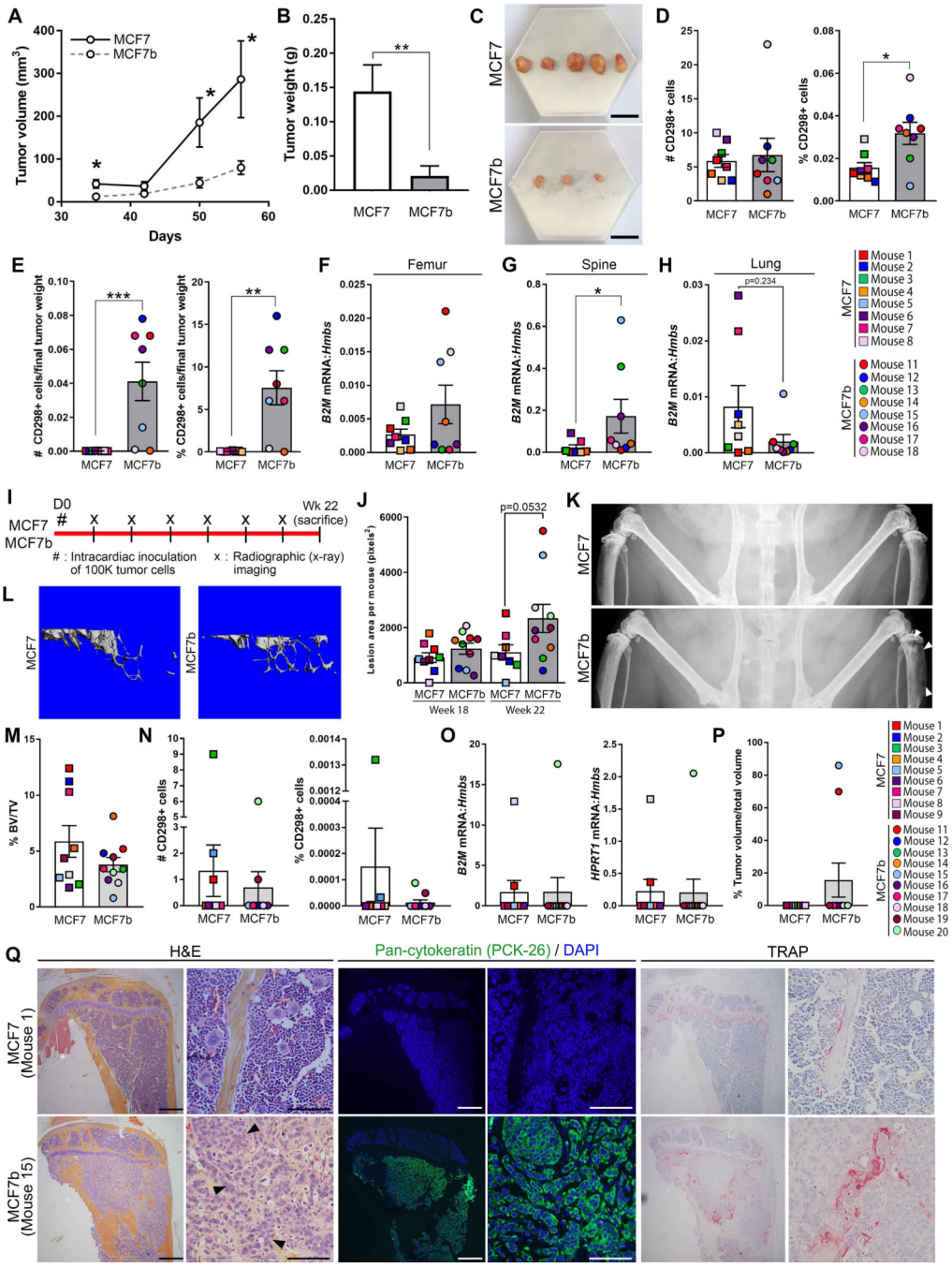

Figure 3. MCF7b cells are primed to disseminate and grow in the bone.

(A) Tumor volume by caliper measurements over 55 days following injection of MCF7 and MCF7b cells into the mammary fat pad with exogenous estrogen supplementation. n=10 mice injected per group. (B) Final tumor weight per mouse after sacrifice (n=8 mice per group at sacrifice). (C) Representative images of primary tumors collected from mice described in (B). (D) Quantitation of total number and percent of CD298+ tumor cells detected by flow cytometry in the bone marrow of mice described in (B). (E) Normalization of data from (D) to final tumor weight (B). (F-H) qPCR analysis of whole (F) femur, (G)

spine, or (H) lung homogenates for human *B2M* normalized to mouse *Hmbs* (housekeeping gene) from mice described in (B). (I) Schematic of experimental timeline from intracardiac inoculation of MCF7 and MCF7b cells (indicated by pound symbol) without exogenous estrogen supplementation, radiographic imaging (indicated by x), and sacrifice. n=9 MCF7-inoculated mice and n=10 MCF7b-inoculated mice at sacrifice. (J) Radiographic assessment of total lesion area per mouse over time of mice described in (I). (K) Representative radiographic images at week 22 of mice described in (I). (L) Representative microCT images of mice described in (I) MCF7-inoculated mouse = mouse 4, MCF7b-inoculated mouse = mouse 17, chosen since these two mice are close to the average % BV/TV for each group. (M) Bone volume/total volume (%BV/TV) from microCT analysis from (I). (N) Quantitation of total number and percent of CD298+ tumor cells detected by flow cytometry in the bone marrow of mice described in (I). (O) qPCR of whole bone homogenate for human *B2M* or human *HPRT1* normalized to mouse *Hmbs* (housekeeping gene) from mice described in (I). (P) Histomorphometric analysis of tumor volume/total volume from mice described in (I). (Q) Representative hematoxylin and eosin (H&E), pan-cytokeratin and DAPI, or tartrate-resistant acid phosphatase (TRAP) staining of tibiae from mice described in (I). All panels, left = 4X, right = 40X of the same tibia. Scale bars = 500μm (left panel), 100μm (right panel). A: Two-way ANOVA with Tukey's multiple comparisons test. B, D-H, J: Mann-Whitney test. Bar graphs indicate mean + standard error of the mean.

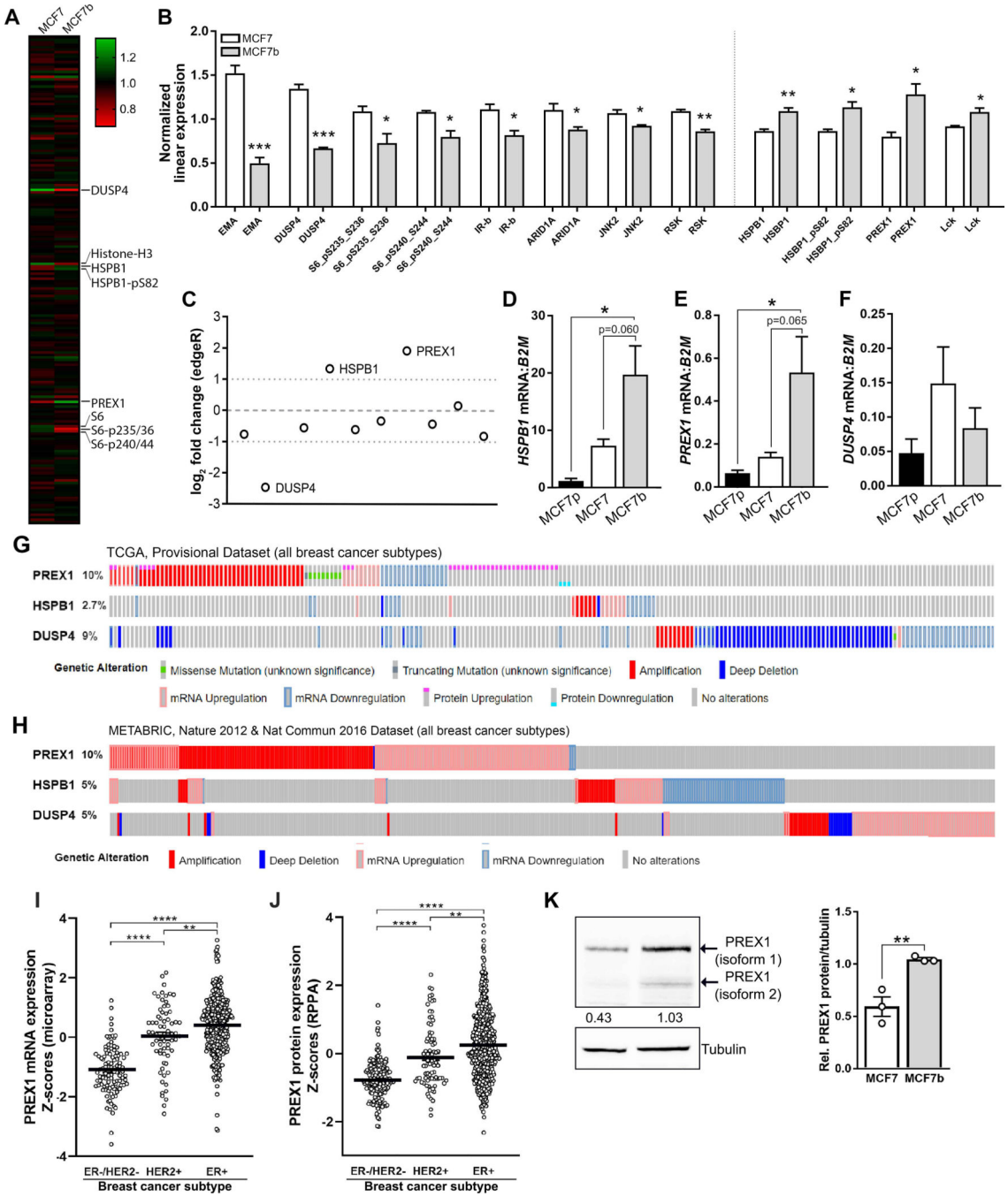

Figure 4. Molecular profiling identifies PREX1 upregulation in MCF7b cells.

(A) Heatmap representing the normalized linear protein expression of the 296 total and phospho-specific proteins evaluated by RPPA in MCF7 and MCF7b cells. (B) Normalized linear protein expression of the significantly altered total and phospho-proteins in MCF7b cells. (C) Log2 fold change in mRNA of the significantly altered proteins from (B) as assessed by RNA-sequencing of MCF7 and MCF7b cells. (D-F) qPCR of parental (MCF7p), MCF7, and MCF7b cells for (D) *HSPB1*, (E) *PREX1*, and (F) *DUSP4* mRNA normalized to *B2M* (housekeeping gene). (G, H) Genetic alterations of *PREX1*, *HSPB1*, and *DUSP4* in

breast cancer patients of all breast cancer subtypes from the (G) TCGA Provisional dataset and (H) METABRIC, Nature 2012, & Nat Comm 2016 dataset. (I, J) Expression of *PREX1* (I) mRNA and (J) protein separated by cancer subtype in patients from the TCGA provisional dataset. (K) Representative western blot for PREX1 and tubulin in MCF7 and MCF7b cells and quantitation of three western blots. B, K: Mann-Whitney test. D-F, I, J: One-way ANOVA with Sidak's multiple comparisons test. *p<0.05, **p<0.01, ***p<0.001. A-F, K: n= three independent biological replicates. Bar graphs indicate mean + standard error of the mean.

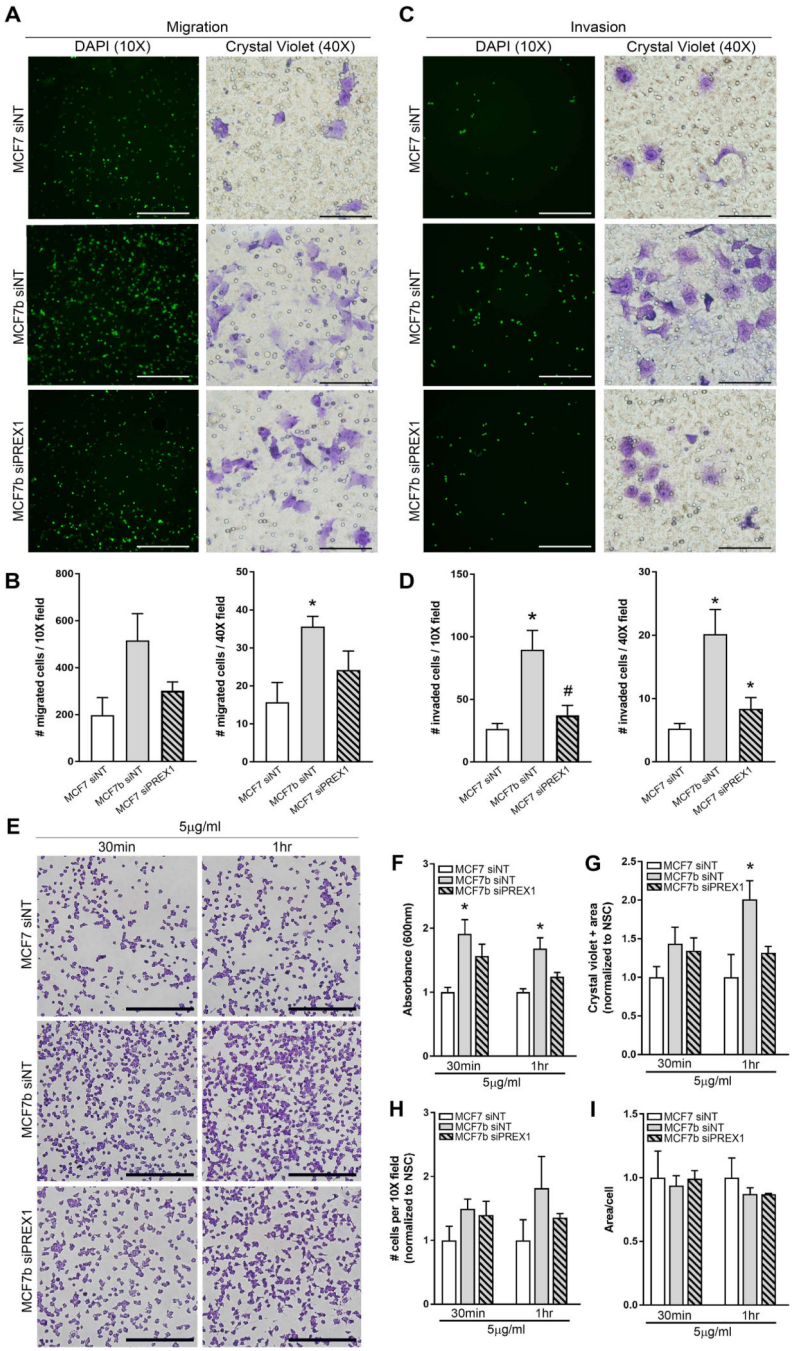

Figure 5. PREX1 knockdown rescues MCF7b invasive properties.

(A) Representative images of MCF7 and MCF7b transfected with a non-silencing siRNA (siNT) or PREX1-targeting siRNAs (siPREX1) evaluated for cell migration by DAPI (green pseudocolor) or crystal violet staining. Left panel = 10X, scale bar = 500μm; right panel = 40X, scale bar = 100μm. (B) Quantitation of the number of migrated cells per 10X or 40X field from (A). (C) Representative images of cell invasion of MCF7 and MCF7b transfected with a non-silencing siRNA (siNT) or PREX1-targeting siRNA (siPREX1) assessed as in (A). (D) Quantitation of the number of invaded cells per 10X or 40X field from (C). (E)

Representative images of adherent MCF7 and MCF7b cells transfected with non-targeting siRNAs (siNT) or PREX1-targeting siRNAs (siPREX) incubated on 5μg/ml fibronectin for 30 minutes or 1 hour. All panels = 10X, scale bar = 500μm. (F) Crystal Violet absorbance measurements at 600nm to assess adherent cells from (E). (G-I) Quantitation of (G) total crystal violet area per field, (H) number of cells per field, and (I) area per cell from (E). B, D: One-way ANOVA with Sidak's multiple comparisons test. *$p<0.05$ compared to MCF7 siNT. #$p<0.05$ compared to MCF7b siNT. F-I: One-way ANOVA with Sidak's multiple comparisons test. *$p<0.05$ compared to MCF7 siNT. n= three independent biological replicates. Bar graphs indicate mean + standard error of the mean.

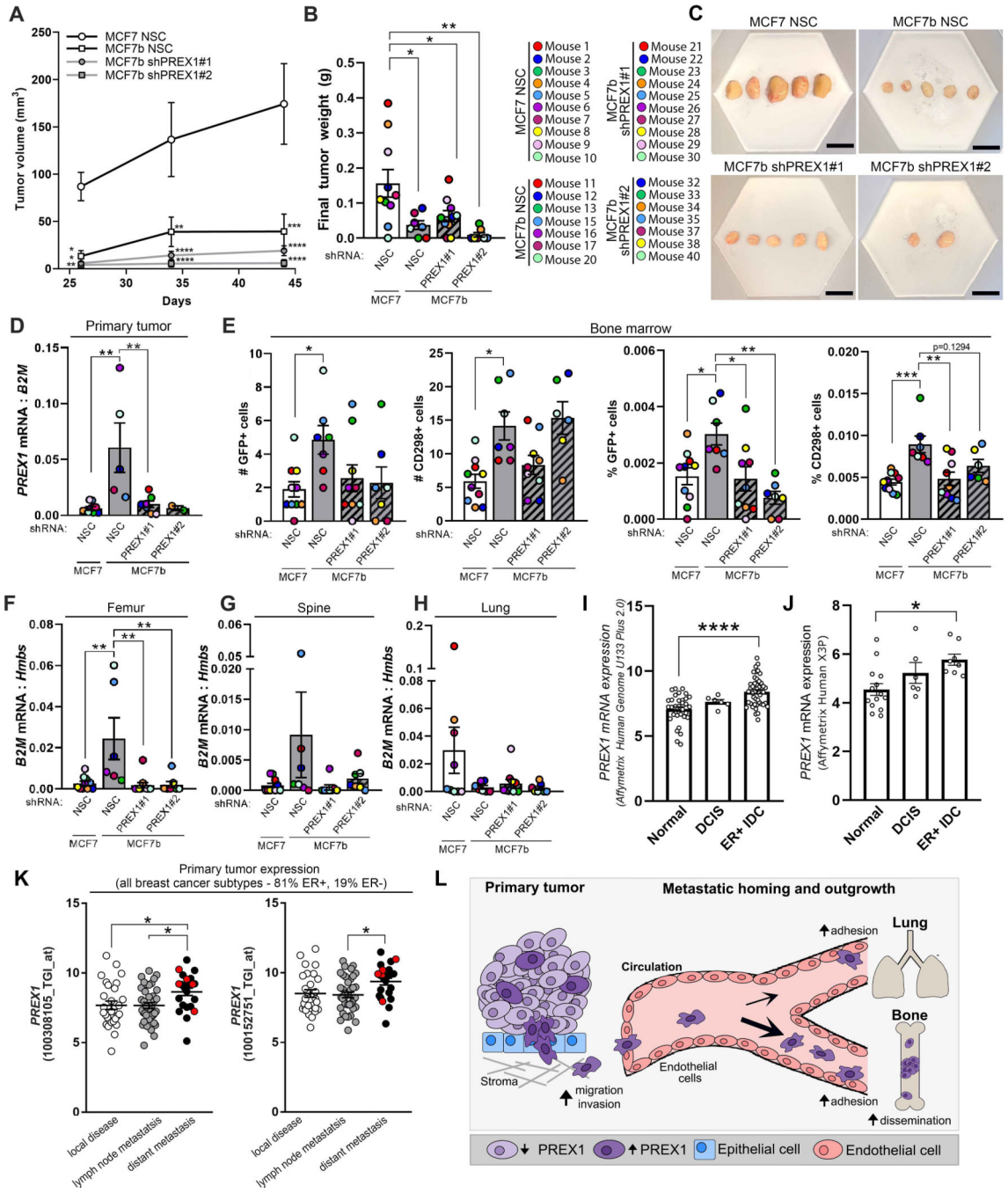

Figure 6. Loss of PREX1 ablates spontaneous dissemination of MCF7b cells to the bone.

(A) Tumor volume by caliper measurements over 44 days following injection of MCF7 NSC (n=10), MCF7b NSC (n=7), or MCF7b shPREX1 (shPREX1#1 (n=10) and shPREX1#2 (n=7) = two independent shRNAs) cells into the mammary fat pad. (B) Final tumor weight per mouse after sacrifice of mice described in (A). (C) Representative images of primary tumors collected from mice described in (A). (D) qPCR of *PREX1* expression in primary tumors isolated from mice described in (A). (E) Quantitation of total number and percent of GFP+ or CD298+ tumor cells detected by flow cytometry in the bone marrow of mice

described in (A). (F-H) qPCR analysis of whole (F) femur, (G) spine, or (H) lung homogenates for human *B2M* normalized to mouse *Hmbs* (housekeeping gene) from mice described in (A). (I, J) *PREX1* mRNA expression in normal, ductal carcinoma in situ (DCIS), and ER+ invasive ductal carcinoma (IDC) patient samples from (I) GSE29044 and (J) GSE14548 datasets. (K) Analysis of *PREX1* mRNA expression in primary breast tumors (81% ER+, 19% ER-) from patients with local disease, lymph node metastases, or distant metastases (GSE46141 dataset). (L) Working model for enhanced metastatic potential of MCF7b cells driven by PREX1 upregulation resulting in increased tumor cell dissemination to the bone. A: Two-way ANOVA with Tukey's multiple comparisons test. B, D-K: One-way ANOVA with Sidak's multiple comparisons test. *$p<0.05$, **$p<0.01$, ***$p<0.001$, ****$p<0.0001$. Bar graphs indicate mean + standard error of the mean.